

Treating Motion as Option with Output Selection for Unsupervised Video Object Segmentation

Suhwan Cho Minhyeok Lee Jungho Lee MyeongAh Cho Sangyoun Lee

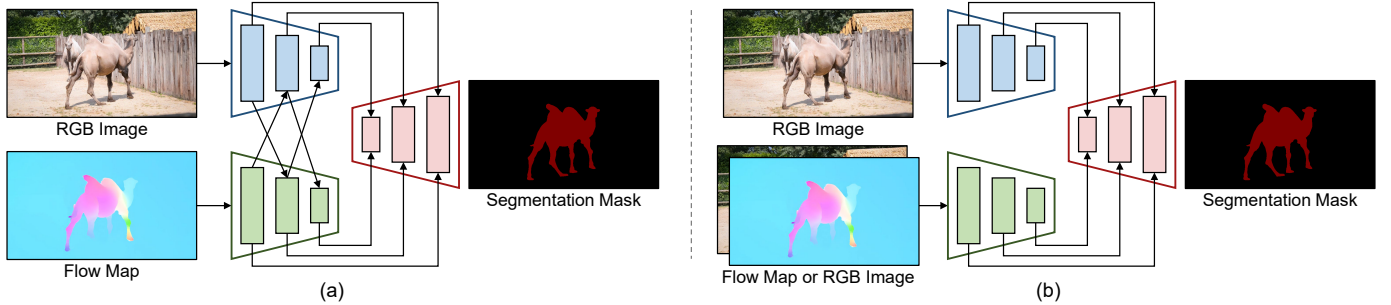


Fig. 1. Visualized comparison of (a) a conventional two-stream VOS network and (b) our proposed motion-as-option network. Unlike existing methods, the motion-as-option network can deal with both RGB images and optical flow maps as its motion input.

Abstract—Unsupervised video object segmentation (VOS) is a task that aims to detect the most salient object in a video without external guidance about the object. To leverage the property that salient objects usually have distinctive movements compared to the background, recent methods collaboratively use motion cues extracted from optical flow maps with appearance cues extracted from RGB images. However, as optical flow maps are usually very relevant to segmentation masks, the network is easy to be learned overly dependent on the motion cues during network training. As a result, such two-stream approaches are vulnerable to confusing motion cues, making their prediction unstable. To relieve this issue, we design a novel motion-as-option network by treating motion cues as optional. During network training, RGB images are randomly provided to the motion encoder instead of optical flow maps, to implicitly reduce motion dependency of the network. As the learned motion encoder can deal with both RGB images and optical flow maps, two different predictions can be generated depending on which source information is used as motion input. In order to fully exploit this property, we also propose an adaptive output selection algorithm to adopt optimal prediction result at test time. Our proposed approach affords state-of-the-art performance on all public benchmark datasets, even maintaining real-time inference speed. Code and models are available at <https://github.com/suhwan-cho/TMO>.

Index Terms—Video object segmentation, Salient object detection, Optical flow estimation, Deep neural networks

I. INTRODUCTION

VIDEO object segmentation (VOS) is a fundamental computer vision task, where the aim is to detect the most

Manuscript received xx xx 2023; revised xx xx 2023; accepted xx xx 2023. Date of publication xx xx 2023; date of current version xx xx 2023. This work was supported by KRIT-Grant funded by Defense Acquisition Program Administration (DAPA) (20-102-E00-013).

Suhwan Cho, Minhyeok Lee, Jungho Lee, and Sangyoun Lee are with the School of Electrical and Electronic Engineering, Yonsei University, Seoul 03722, Korea. MyeongAh Cho is with the Department of Software Convergence, Kyung Hee University, Yongin 17104, Korea.

This work is extended from the preliminary exploration, “Treating Motion as Option to Reduce Motion Dependency in Unsupervised Video Object Segmentation”, presented in *Proceedings of the IEEE/CVF Winter Conference on Applications of Computer Vision*, 2023, pp. 5140-5149.

salient object in a video sequence at the pixel level. Owing to its powerful usefulness for real-world applications, including robotics, video editing, video surveillance, sports analytics, and autonomous driving, it has been widely adopted in many vision systems. Based on the external guidance about the target object, VOS is divided into various subcategories: semi-supervised VOS if initial mask is given; unsupervised VOS if no guidance is given; interactive VOS if scribbles are given; referring VOS if language guidance is given. Among them, we focus on the unsupervised setting, which is also known as zero-shot VOS. As there is no guidance about the object in unsupervised VOS, the task consists of automatically defining the salient object and consistently segmenting that object within the given video sequence.

Considering that salient objects usually have different movements with the background, recent approaches for unsupervised VOS use motion cues extracted optical flow maps in addition to appearance cues extracted from RGB images. Then, the features obtained from respective cues are fused during the embedding process with mutual guidance to each other, as shown in Figure 1 (a). For instance, MATNet [1] adopts a two-stream interleaved encoder, which allows the transition of attentive motion features to enhance appearance features. FSNet [2] proposes a relational cross-attention module to extract discriminative features from appearance and motion cues, and ensure the mutual restraint between each other. AMC-Net [3] introduces a co-attention gate module on the bilateral encoder branches to formulate co-attention scores for balancing the contributions of multi-modality features. Additionally, HFAN [4] proposes a hierarchical mechanism to align and fuse appearance and motion features. However, they are susceptible to low-quality optical flow maps as their network structures are strongly dependent on motion cues.

To overcome this limitation, we design a novel motion-as-option network with simple encoder-decoder architecture that operates regardless of motion availability, as shown in

Figure 1 (b). The two different encoders extract semantic features from appearance input and motion input, while the decoder produces an object segmentation mask by incorporating the embedded features and decoding them. In contrast to the existing two-stream VOS approaches, the motion stream is randomly turned on or off during the network training. If it is turned on, optical flow maps are used as motion input, i.e., both appearance cues and motion cues are used for mask prediction. If it is turned off, RGB images are used as motion input, i.e., only appearance cues are used for mask prediction. As the motion cues, which are very relevant to segmentation masks, are not always provided during training, the network becomes less dependent on motion encoder. This significantly increases robustness of motion-as-option network against confusing optical flow maps during inference.

In order to learn the proposed motion-as-option network to meet our network design goal, we need to prepare the training samples both with and without optical flow maps. A straightforward approach to accomplish this is intentionally discarding optical flow maps in VOS training samples. However, to maximize the property of motion-as-option network that optical flow maps are not always required, we additionally adopt salient object detection (SOD) samples to learn the network with larger amount of data. When VOS samples are used as training data, optical flow maps are fed into the motion encoder, and whereas when SOD samples are used as training data, RGB images are fed into the motion encoder. The proposed collaborative network learning strategy is carefully designed for the proposed motion-as-option network and thus can greatly increase its ability.

After trained with collaborative learning strategy, the motion-as-option network can deal with both RGB images and optical flow maps as motion input. Therefore, during inference, it can generate two different predictions depending on which domain is used as motion input. In order to automatically adopt optimal source information, we also propose an output selection algorithm. For each frame, we calculate and compare overall confidence scores of two outputs, and select one as a final output based on the calculated scores. Compared to conventional soft ensemble methods, our selection algorithm is proven to be more effective for motion-as-option network.

On public benchmark datasets for unsupervised VOS, i.e., DAVIS 2016 [5] validation set, FBMS [6] test set, YouTube-Objects [7] dataset, and Long-Videos [8] dataset, our approach achieves state-of-the-art performance, while maintaining real-time inference speed. Each proposed component is also demonstrated to be effective by extensive analysis. We believe that our proposed simple, fast, and strong solution takes a meaningful step toward useful and applicable VOS system, and can serve as a solid baseline for future VOS research.

The summary of our contributions is as follows:

- We propose a motion-as-option network that optionally leverages motion cues to reduce motion dependency of the network. As it uses motion cues as optional, it can also run without optical flow maps.
- We propose a collaborative network learning strategy to effectively learn the proposed network by leveraging its unique property that motion cues are not always required.

- We propose a novel output selection algorithm for motion-as-option network that adaptively selects optimal prediction result based on confidence score calculation.
- While maintaining a simple architecture and fast inference speed, our proposed approach achieves state-of-the-art performance on all benchmark datasets.

II. RELATED WORK

Temporal coherence. In video sequences, different frames usually share similar visual contents that are highly related to each other. Some early methods for unsupervised VOS have exploited this “locality” in a video, which means that salient objects should appear in every frame of a video. COSNet [9] proposes a global co-attention mechanism to attend to the frequently coherent regions among video frames from a holistic viewpoint. AGNN [10] employs graph neural networks to build a fully connected graph, where each frame is regarded as node and the relations between the frames as edges. After iterative update process based on parametric message passing, a complete understanding of video content can be obtained. DFNet [11] generates the inherent long-term correlation between different video frames by revealing feature distribution from a global perspective. AD-Net [12] and F2Net [13] reconsider long-term dependencies within a video sequence by calculating dense correspondences between reference frame pixels and query frame pixels. IMP [14] combines SOD algorithm and semi-supervised VOS algorithm to iteratively propagate the predicted mask of one frame to other remaining frames. As multiple frames are required to obtain frame-level coherence in these methods, each separate frame cannot be inferred independently.

Motion information. Inspired by the observation that salient objects usually have distinctive movements that can be easily distinguished from the background, recent methods have exploited optical flow maps obtained from pre-trained flow estimation models in addition to RGB images. MATNet [1] proposes a two-stream interleaved encoder architecture to use motion cues for improving appearance cues for the first time. RTNet [15] tackles the problem that optical flow maps are sometimes too noisy, which causes misguidance about salient object. To address this problem, a reciprocal transformation network is proposed to discover the object by correlating intra-frame contrast, motion cues, and temporal coherence within a video. FSNet [2] uses a full-duplex strategy to effectively exchange information between appearance and motion cues. A relational cross-attention module is proposed to ensure the mutual restraint between appearance and motion cues based on bi-directional message propagation across embedding spaces. TransportNet [16] suppresses the distracting noises using optimal structural matching via Sinkhorn algorithm. AMC-Net [3] evaluates the importance of appearance and motion input, and weights their features to modulate the influences of each modality. HFAN [4] and HCPN [17] leverage a hierarchical mechanism to align and fuse appearance and motion features of different embedding levels independently. In most two-stream approaches, each frame is processed independently, i.e., only an RGB image and an optical flow map are required for

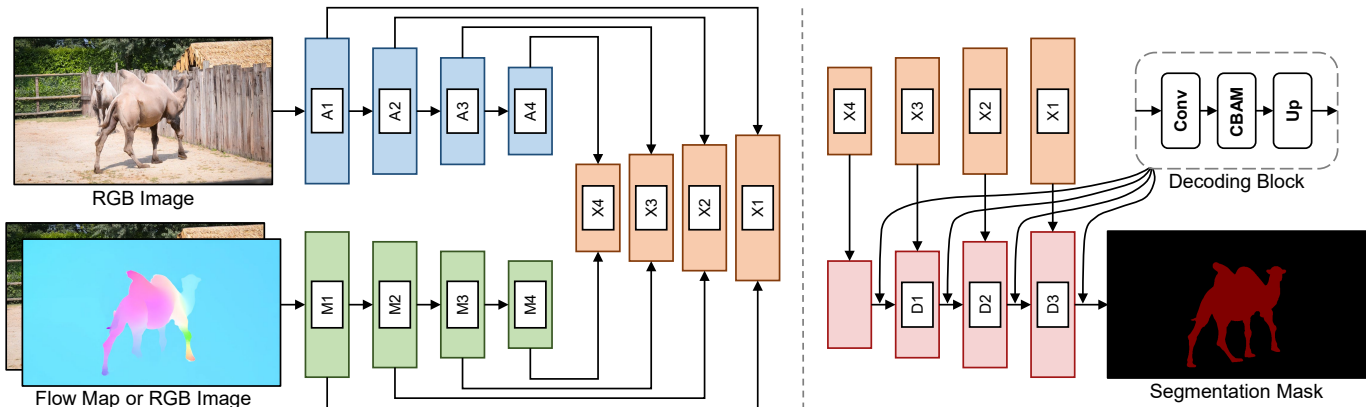


Fig. 2. Architecture of our proposed network. If we choose to leverage motion cues, an optical flow map is used as motion input, whereas if we choose not to leverage motion cues, an RGB image is used as motion input. After obtaining appearance features and motion features from the encoders, respective features are first fused with each other and then gradually decoded to predict the final segmentation mask.

inference. However, as they are highly dependent on motion cues, stable prediction cannot be achieved when confusing optical flow maps are provided.

Network learning strategy. One of the most significant barriers in unsupervised VOS is that training data is not sufficient compared to other vision tasks, which often leads to network overfitting. To relieve this issue, some existing methods have adopted external training samples from other vision tasks. AGS [18] exploits image SOD datasets, DUT [19] and PASCAL-S [20], both of which provide static gaze data. COSNet and AGNN use segmentation models pre-trained on MSRA10K [21] and DUT as their backbone networks, and fine-tune them on the VOS dataset, DAVIS 2016 [5]. RTNet and FSNet use DUTS [22] to pre-train the networks on SOD training samples. IMP [14] uses a semi-supervised VOS model which is trained on large segmentation datasets, such as COCO [23] and YouTube-VOS 2018 [24].

Model Ensemble. Various ensemble methods have been suggested to reduce the variance and increase the accuracy of the models [25]. The idea behind ensemble methods is to combine multiple models to achieve better performance than any single model alone. With the rise of deep learning, they have been adapted for various vision tasks using deep neural networks. One example is human action recognition, which aims to categorize action classes by receiving human video data. Shift-GCN [26], HD-GCN [27], and STC-Net [28] employ weighted ensemble method at test time to consider multiple prediction results obtained from different input streams. Ensemble methods are also widely used in segmentation tasks including semi-supervised VOS and unsupervised VOS. A common approach is to obtain various pixel-level predictions by augmenting input images. CFBI [29], RPCMVOS [30], and HFAN intentionally resize and flip input images in order to increase the number of predictions. In terms of exploiting multiple outputs at the same time, our proposed adaptive output selection algorithm is quite similar to these ensemble methods. In Section IV-C, we demonstrate the superiority of our proposed method compared to the conventional ensemble methods under our settings.

III. APPROACH

A. Problem Formulation

Given an input video sequence, unsupervised VOS model aims to predict segmentation masks of a salient object. Following recent approaches, we generate optical flow maps using a pre-trained optical flow estimation model and use the extracted motion cues in addition to appearance cues. Note that 2-channel motion vectors are converted to 3-channel RGB values before feature embedding. Similar to existing two-stream methods, such as MATNet [1] and FSNet [2], input video is processed frame-by-frame in our method. When inferring i -th frame segmentation mask, only i -th frame RGB image and i -th frame optical flow map are used.

B. Motion-as-Option Network

To reduce vulnerability of existing two-stream architecture against low-quality or confusing optical flow maps, we propose a novel motion-as-option network that operates regardless of motion availability and therefore is not dependent on motion cues. We visualize the architecture of our proposed motion-as-option network in Figure 2.

Separate encoders. Inspired by the observation that RGB images and optical flow maps have different advantages that can complement each other, existing two-stream methods employ two deeply connected encoders for embedding respective source information. During the encoding process, appearance features and motion features exchange their information, imposing constraints on each other. As respective features cannot be embedded separately, those dual encoders can be regarded as a single encoder that takes an RGB image and an optical flow map as its input. Therefore, they are very dependent on motion cues obtained from optical flow maps in its nature, which causes critical errors when low-quality or confusing optical flow maps are provided as input.

Unlike the existing two-stream methods, we use two completely separated encoders to embed appearance and motion features independently. In other words, during the feature embedding process, there is no interaction between appearance

encoder and motion encoder. Let us denote appearance features as $\{A_k\}_{k=1}^K$ and motion features as $\{M_k\}_{k=1}^K$, where K is the number of blocks in the respective encoders and a higher k value indicates higher-level features. The appearance features are embedded from RGB images, whereas the motion features are embedded from either RGB images or optical flow maps. Then, by simply summing appearance and motion features of each level, fused features $\{X_k\}_{k=1}^K$ can be defined as

$$X_k = A_k + M_k . \quad (1)$$

In our encoder, appearance features and motion features are independently embedded and then fused. This makes our network robust against confusing motion cues, as potential negative influence of motion features on the appearance features can be prevented in advance. In addition, considering that the motion encoder takes both RGB images and optical flow maps as its input, network overfitting to explicit optical flow maps can also be prevented. This also makes motion-as-option network not always requiring optical flow maps during inference, increasing usability of the network.

Decoder. With the fused features, the decoder generates segmentation mask of the salient object. In order to convert low-resolution features to high-resolution masks, the fused features are gradually refined using multiple decoding blocks that are similarly designed to those of TBD [31]. Each decoding block consists of a convolutional layer that blends features from different embedding levels, a CBAM [32] layer that reinforces feature representations, and an upsampling layer that increases feature resolution. Assuming Ψ_k indicates the k -th decoding block, where a higher k value indicates higher resolution, decoded features $\{D_k\}_{k=1}^K$ can be obtained as

$$D_k = \begin{cases} \Psi_k(X_{K-k+1}) & k = 1 \\ \Psi_k(D_{k-1} \oplus X_{K-k+1}) & \text{otherwise} , \end{cases} \quad (2)$$

where \oplus indicates channel concatenation. After K decoding blocks, the final segmentation mask can be obtained after pixel value quantization to 0 or 1.

C. Collaborative Learning Strategy

In order to learn the proposed motion-as-option network in accordance with our network design goal, training samples with and without optical flow maps should be prepared as training data. A straightforward approach to accomplish this is to intentionally and randomly discard optical flow maps of VOS training samples. However, instead, we additionally adopt SOD samples for network training, to fully leverage the unique property of the motion-as-option network that optical flow maps are not always required.

Although collaboratively leveraging VOS and SOD samples sounds reasonable, it cannot be directly implemented on GPU devices for batch training as they have different formats. To solve this issue, we adopt a simple indexing trick. First, training data samples are randomly sampled from VOS training set and SOD training set, based on a pre-defined sampling ratio. Each VOS sample consists of an RGB image, an optical flow map, and an object segmentation mask. In contrast, each SOD sample consists of an RGB image and an object segmentation

mask. Then, to ensure that the samples have the same format, we generate void tensors for the SOD samples and regard them as optical flow maps. Finally, to verify the validity of the prepared optical flow maps, a motion validity index is allocated for each training sample. For VOS and SOD samples, it is set to 1 and 0, respectively. Based on this trick, feature embedding process is implemented as shown in Code Listing 1. By adopting collaborative network learning strategy, motion-as-option network can obtain more comprehensive knowledge compared to when VOS training samples are used alone.

```
# A: appearance features
# M: motion features
# X: fused features
A, M = {}, {}

# image: (Bx3xHxW), RGB images
# extract appearance features
a = image
for k in K:
    A[k] = app_block_k(a)
    a = A[k]

# i: (Bx1x1x1), motion validity indices
# flow: (Bx3xHxW), optical flow maps
# extract motion features
m = i * flow + (1 - i) * image
for k in K:
    M[k] = mo_block_k(m)
    m = M[k]

# generate fused features
for k in K:
    X[k] = A[k] + M[k]
```

Code Listing 1. Feature embedding process with indexing trick.

D. Adaptive Output Selection

After training motion-as-option network using collaborative learning strategy, the motion encoder can deal with both RGB images and optical flow maps as it has seen both information during network training. In other words, the network can generate two different outputs when tested on VOS samples depending on which source information is provided to the motion encoder, i.e., an RGB image or an optical flow map. Based on the preliminary exploration, TMO [33], that providing optical flow maps to motion encoder does not always show better results than providing RGB images, we design a novel adaptive output selection algorithm to adopt optimal source information for final prediction. We visualize overall pipeline of adaptive output selection algorithm in Figure 3.

Let us denote output logit map obtained from the motion-as-option network as $\sigma \in \mathbb{R}^{2 \times H \times W}$, where the first and second channels indicate background and foreground scores, respectively. Then, we can obtain foreground prediction map $\omega \in [0, 1]^{H \times W}$ as

$$\omega^p = \frac{\exp(\sigma_{FG}^p)}{\exp(\sigma_{BG}^p) + \exp(\sigma_{FG}^p)} , \quad (3)$$

where p indicates each pixel location. Then, confidence map $\phi \in [0, h]^{H \times W}$ can be calculated as

$$\phi^p = \begin{cases} h - \omega^p & \omega^p < h \\ \omega^p - 1 + h & \omega^p > 1 - h \\ 0 & \text{otherwise} , \end{cases} \quad (4)$$

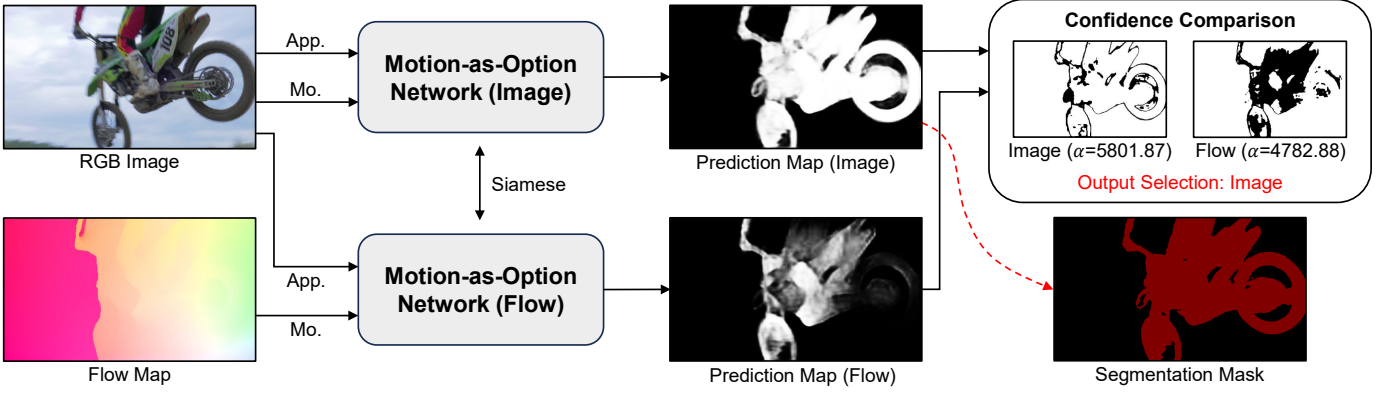


Fig. 3. Visualized pipeline of adaptive output selection algorithm. Motion-as-option network produces two different outputs: one from an RGB image as motion input; the other from an optical flow map as motion input. Then, the final segmentation mask is obtained by evaluating each output based on the overall confidence scores.

where $h \in [0, 0.5]$ is a pre-defined threshold value. Finally, confidence score α can be obtained as

$$\alpha = \sum_p \phi^p. \quad (5)$$

α represents overall confidence score of the network prediction, as it is the sum of clearly distinguishable pixels' degree of certainty (either clear background or clear foreground). By comparing α of different prediction results, we can evaluate which output is more reliable, i.e., which source information is more useful for motion encoder. After selecting the prediction result, final segmentation mask can be generated from ω . For example, in Figure 3, providing an RGB image to motion encoder shows higher α value compared to providing an optical flow map. In this case, final prediction is obtained without using motion cues.

E. Implementation Details

Optical flow map. In order to leverage motion cues in addition to appearance cues, we use optical flow maps as source information. To obtain flow map at frame i , we consider frame i as the starting frame and frame $i+1$ as the target frame. If i is the last frame of a video, frame $i-1$ is considered as the target frame. For optical flow estimation, we use RAFT [34] pre-trained on the Sintel [35] dataset. The flow maps are generated while maintaining original resolution of the data samples. To remove redundant training and testing times, optical flow maps are generated and saved in advance, instead of being estimated in the middle of the system.

Encoder. Similar to recent VOS approaches, we adopt ResNet-101 [36] and MiT-b1 [37] as our backbone encoder. As pixel-level prediction is required, only the first four blocks are detached and used for feature embedding. The features extracted from the k -th block have the scale of $1/2^{k+1}$ compared to the input resolution, where total block number K is 4. To leverage rich feature representations obtained from large number of training samples, both appearance and motion encoders are initialized with the weights learned from ImageNet [38].

Confidence map. To evaluate certainty level of predictions, confidence maps are generated based on foreground prediction maps. During this process, pixels that are not clearly

distinguishable are first filtered out before confidence score calculation. The threshold value h is empirically set to 0.05, but no significant performance difference is observed for different h values.

F. Network Training

Data preparation. To obtain training data diversity and better leverage motion-as-option network's unique property, we adopt both VOS and SOD samples for network training, as described in Section III-C. For the VOS samples, only the DAVIS 2016 [5] training set is employed. Note that FBMS [6] also has a training set but is not used for network training following common protocol in unsupervised VOS. For the SOD samples, we adopt both DUTS [22] training and testing sets. The training data for our method is randomly sampled from VOS and SOD samples with fixed probabilities of 25% and 75%, respectively.

Training details. For all the training stages, we resize RGB images, optical flow maps, and segmentation masks to 384×384 resolution. As the resizing method, we use bicubic interpolation for both RGB images and optical flow maps. To ensure that the resized segmentation masks have the values of either 0 or 1, nearest interpolation is used for VOS samples while bicubic interpolation and value quantization are sequentially applied to SOD samples. As the training objective, we adopt conventional cross-entropy loss function. In addition, we use Adam optimizer [39] with the learning rate of $1e-5$ without learning rate decay. The batch size is set to 16. Following recent VOS algorithms, such as STM [40], KMN [41], CFBI [29], and BMVOS [42], we freeze all batch normalization layers [43] during network training. For all model versions, network training is implemented on two GeForce RTX 2080 Ti GPUs and takes less than 20 hours.

IV. EXPERIMENTS

In Section IV-A, we first describe the datasets used in this study. Evaluation metrics to quantitatively assess the model performance are described in Section IV-B. Then, we thoroughly validate the effectiveness of each proposed component by conducting an extensive analysis in Section IV-C.

In Section IV-D and Section IV-E, we compare our proposed approach to other state-of-the-art methods quantitatively and qualitatively. Our baseline method is abbreviated as TMO. If adaptive output selection algorithm is applied on top of it, our method is abbreviated as TMO++.

A. Datasets

To confirm the validity of our proposed approach, we use five datasets that are widely adopted for unsupervised VOS. For network training, DUTS [22] and DAVIS 2016 [5] are used. For network testing, DAVIS 2016, FBMS [6], YouTube-Objects [7], and Long-Videos [8] are used.

DUTS. DUTS is one of the largest SOD datasets, comprising 10,553 training images and 5,019 testing images, each with densely annotated ground truth segmentation masks. It is only used for network training in our approach.

DAVIS 2016. DAVIS 2016 is one of the most popular datasets for VOS-related tasks. It contains 30 training videos and 20 validation videos that only contain single-object scenarios. It is used for both network training and testing.

FBMS. FBMS comprises 59 video sequences, and a total of 720 frames are annotated. In some sequences, multiple objects are annotated as salient objects. Following common protocol in unsupervised VOS, it is only used for network testing.

YouTube-Objects. YouTube-Objects dataset is composed of videos collected from YouTube and contains 10 object classes. As there is no training set / test set separation, it is only used for network testing.

Long-Videos. Long-Videos is a dataset obtained for real-world tasks, where each video sequence contains at least 1,400 frames. It is originally designed for semi-supervised VOS, but we use it for performance validation as main objects continuously appear in every sequence.

B. Evaluation Metrics

In order to measure the segmentation performance of unsupervised VOS methods, we use evaluation protocols used in general image segmentation tasks. There are two kinds of metrics widely adopted: \mathcal{J} and \mathcal{F} . \mathcal{J} metric is equal to naive intersection-over-union (IoU), and is used to measure the region similarity. It can be represented as

$$\mathcal{J} = \left| \frac{M_{gt} \cap M_{pred}}{M_{gt} \cup M_{pred}} \right|, \quad (6)$$

where M_{gt} and M_{pred} denote the ground truth and predicted segmentation masks, respectively. \mathcal{F} metric is similar to \mathcal{J} metric, but is calculated only for object boundaries. It can be obtained as

$$\text{Precision} = \left| \frac{M_{gt} \cap M_{pred}}{M_{pred}} \right|, \quad (7)$$

$$\text{Recall} = \left| \frac{M_{gt} \cap M_{pred}}{M_{gt}} \right|, \quad (8)$$

$$\mathcal{F} = \frac{2 \times \text{Precision} \times \text{Recall}}{\text{Precision} + \text{Recall}}. \quad (9)$$

TABLE I

ABLATION STUDY ON NETWORK TRAINING AND TESTING PROTOCOLS. TRAINING INDICATES WHICH TRAINING PROTOCOL IS ADOPTED. ME DENOTES SOURCE INFORMATION FOR MOTION ENCODER. D, F, AND Y DENOTE DAVIS 2016 VALIDATION SET, FBMS TEST SET, AND YOUTUBE-OBJECTS DATASET, RESPECTIVELY.

Version	Training	ME (Test)	D	F	Y
I	VOS	Flow	76.5	59.2	57.2
II	SOD \rightarrow VOS	Flow	82.1	74.7	63.0
III	VOS & SOD	Flow	86.1	79.9	71.5
IV	VOS	Image	63.7	52.8	52.6
V	SOD \rightarrow VOS	Image	73.0	76.8	69.3
VI	VOS & SOD	Image	80.0	80.0	73.1

TABLE II

ABLATION STUDY ON NETWORK TRAINING AND TESTING PROTOCOLS. ME DENOTES SOURCE INFORMATION FOR MOTION ENCODER. D, F, AND Y DENOTE DAVIS 2016 VALIDATION SET, FBMS TEST SET, AND YOUTUBE-OBJECTS DATASET, RESPECTIVELY.

Version	ME (Train)	ME (Test)	D	F	Y
I	Flow Always	Flow	76.5	59.2	57.2
II	Flow or Image	Flow	75.7	59.9	60.0
III	Flow Always	Image	63.7	52.8	52.6
IV	Flow or Image	Image	72.7	59.8	59.6

\mathcal{G} metric, which is the average of \mathcal{J} and \mathcal{F} , is also a widely used metric for evaluating VOS performance.

C. Analysis

In this section, we conduct a thorough analysis with respect to the network training protocols and network testing protocols. As evaluation metrics, \mathcal{G} score is adopted for the DAVIS 2016 [5] validation set, whereas for the FBMS [6] test set and YouTube-Objects [7] dataset, \mathcal{J} score is adopted. Note that we use the model version that uses ResNet-101 [36] as backbone encoders in this section.

Collaborative learning strategy. We validate the effectiveness of our proposed collaborative network learning strategy in terms of training data construction in Table I. As can be seen from version I, network is easily overfitted to the training samples if only VOS samples are adopted for network training. Compared to version II and version III, it shows much lower performance on all datasets. To prevent this overfitting problem, some early works employ SOD samples to pre-train the network and then fine-tune it on VOS samples. For a fair comparison with those methods, we simulate this protocol in version II. Although it shows better performance than version I, performance is still not satisfactory, especially on the YouTube-Objects dataset. This is because the network forgets the general knowledge learned from SOD samples and is fitted to the small number of VOS samples during the fine-tuning stage. In contrast, if our proposed collaborative network learning strategy is adopted as in version III, the model achieves the highest performance on all datasets. Specifically, significant performance improvements are observed on the FBMS test set and YouTube-Objects dataset. As VOS and SOD training samples are consistently provided for network

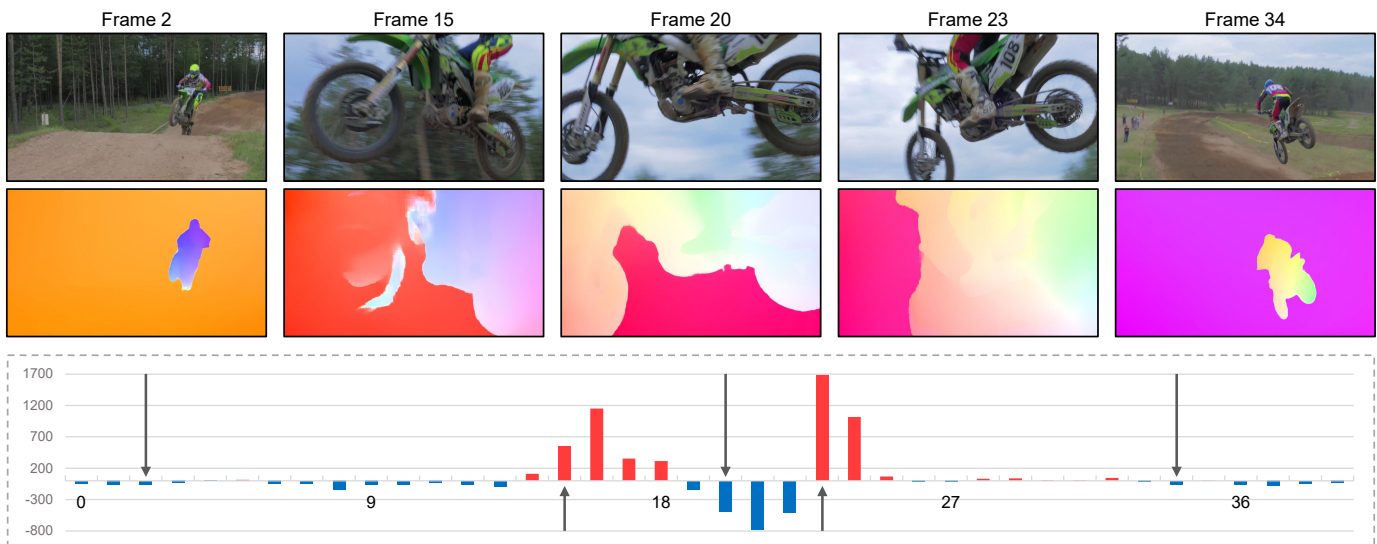


Fig. 4. Visualized confidence scores of a sample video sequence. x-axis is frame number and y-axis is difference of confidence scores between using RGB images as motion input and optical flow maps as motion input. Positive difference values indicate that using RGB images shows higher confidence scores compared to using optical flow maps, and vice versa.

training, the network can learn high-quality fine knowledge from VOS samples, while at the same time learning comprehensive knowledge from large number of SOD samples.

In Table II, we quantitatively compare the model versions with and without intentional motion cue removal during training. For a fair comparison, all model versions are trained only with the DAVIS 2016 training set. It can be observed that version I shows slightly better performance on the DAVIS 2016 validation set, but version II shows better generalization ability compared to version I. This indicates that learning the motion encoder with both RGB images and optical flow maps makes the network more robust to various scenarios, compared to only optical flow maps are used.

Motion dependency. We also report the performance of different model versions when RGB images are fed into the motion encoder at testing stage. As can be seen from version IV, version V, and version VI in Table I, the performance on the DAVIS 2016 validation set decreases when RGB images are used as motion input compared to when optical flow maps are adopted as motion input. Among the model versions, version VI shows the smallest decrement on performance, showing its low motion dependency. Interestingly, on FBMS test set and YouTube-Objects dataset, the use of motion cues is not as effective as on the DAVIS validation set. In some cases, not using motion cues even raise the performance of the model. Specifically, version VI yields 0.1% and 1.6% higher prediction scores compared to version III on the FBMS test set and YouTube-Objects dataset, respectively. This observation also backups the need for treating motion as option, as using motion cues are not always helpful for better prediction.

Output selection. As can be seen from Table I and Table II, using motion cues is not always helpful to obtain better performance. In other words, optimal source information for motion encoder varies by situation. If the quality of optical flow maps is high, using optical flow maps as motion input produces better results, whereas if the quality of optical flow

TABLE III
ABLATION STUDY ON NETWORK TESTING PROTOCOL. TESTING INDICATES WHICH TESTING PROTOCOL IS ADOPTED. D, F, AND Y DENOTE DAVIS 2016 VALIDATION SET, FBMS TEST SET, AND YOUTUBE-OBJECTS DATASET, RESPECTIVELY.

Version	Description	Testing	D	F	Y
I	TMO [33]	Flow Only	86.1	79.9	71.5
II	-	Image Only	80.0	80.0	73.1
III	-	Input Fusion	83.7	80.3	72.8
IV	-	Feature Fusion	84.6	80.9	73.3
V	-	Output Fusion	84.7	81.0	73.2
VI	TMO++	Output Selection	86.1	81.2	73.1

TABLE IV
QUANTITATIVE ANALYSIS ON ADAPTIVE OUTPUT SELECTION. IMAGE AND FLOW INDICATE THE SELECTION RATIOS OF RGB IMAGES AND OPTICAL FLOW MAPS AS MOTION INPUT, RESPECTIVELY.

Dataset	Image (%)	Flow (%)
DAVIS 2016 [5]	3.78	96.2
FBMS [6]	37.6	62.4
YouTube-Objects [7]	38.8	61.2

maps is low, using RGB images as motion input produces better results. To select optimal motion input, we propose an adaptive output selection algorithm.

In Figure 4, a sample video sequence is visualized with per-frame confidence score difference. It can be observed that even within a single video sequence, source information showing higher confidence scores keeps changing. For instance, at frame 15 and frame 23, providing an RGB image as motion input achieves higher confidence score than providing an optical flow map, as optical flow maps are quite confusing. Whereas at frame 20, providing an optical flow map to motion encoder yields higher overall confidence score, as the estimated flow map accurately captures edges and structures of the object and thus can provide explicit guidance about the object to

TABLE V
 QUANTITATIVE EVALUATION ON THE DAVIS 2016 VALIDATION SET AND FBMS TEST SET. OF AND PP INDICATE THE USE OF OPTICAL FLOW ESTIMATION MODELS AND POST-PROCESSING TECHNIQUES, RESPECTIVELY. * DENOTES SPEED CALCULATED ON THE SAME HARDWARE.

Method	Publication	Resolution	OF	PP	fps	DAVIS 2016			FBMS
						\mathcal{G}_M	\mathcal{J}_M	\mathcal{F}_M	\mathcal{I}_M
PDB [44]	ECCV'18	473×473		✓	20.0	75.9	77.2	74.5	74.0
MOTAdapt [45]	ICRA'19	-		✓	-	77.3	77.2	77.4	-
AGS [18]	CVPR'19	473×473		✓	10.0	78.6	79.7	77.4	-
COSNet [9]	CVPR'19	473×473		✓	-	80.0	80.5	79.4	75.6
AD-Net [12]	ICCV'19	480×854		✓	4.00	81.1	81.7	80.5	-
AGNN [10]	ICCV'19	473×473		✓	3.57	79.9	80.7	79.1	-
MATNet [1]	AAAI'20	473×473	✓	✓	20.0	81.6	82.4	80.7	76.1
WCS-Net [46]	ECCV'20	320×320			33.3	81.5	82.2	80.7	-
DFNet [11]	ECCV'20	-		✓	3.57	82.6	83.4	81.8	-
3DC-Seg [47]	BMVC'20	480×854		✓	4.55	84.5	84.3	84.7	-
F2Net [13]	AAAI'21	473×473			10.0	83.7	83.1	84.4	77.5
RTNet [15]	CVPR'21	384×672	✓	✓	-	85.2	85.6	84.7	-
FSNet [2]	ICCV'21	352×352	✓	✓	12.5	83.3	83.4	83.1	-
TransportNet [16]	ICCV'21	512×512	✓		12.5	84.8	84.5	85.0	78.7
AMC-Net [3]	ICCV'21	384×384	✓	✓	17.5	84.6	84.5	84.6	76.5
D ² Conv3D [48]	WACV'22	480×854			-	86.0	85.5	86.5	-
IMP [14]	AAAI'22	-			1.79	85.6	84.5	86.7	77.5
HFAN (MiT-b1) [4]	ECCV'22	512×512	✓		18.4*	86.7	86.2	87.1	-
PMN [49]	WACV'23	352×352	✓		-	85.9	85.4	86.4	77.7
HCPN [17]	TIP'23	512×512	✓	✓	2.00	85.6	85.8	85.4	78.3
TMO (RN-101) [33]	WACV'23	384×384	✓		43.2*	86.1	85.6	86.6	79.9
TMO++ (RN-101)		384×384	✓		26.3*	86.1	85.6	86.6	81.2
TMO (MiT-b1) [33]	WACV'23	384×384	✓		66.7*	87.2	86.6	87.8	80.0
TMO++ (MiT-b1)		384×384	✓		39.1*	87.2	<u>86.5</u>	87.8	83.2

the network. The qualitative visual evaluation also accords with the quantitative results, demonstrating effectiveness of the proposed adaptive output selection algorithm.

In Table III, we compare various output processing methods to validate the efficacy of the proposed adaptive output selection algorithm. Version I and version II use single source information for motion encoder, and are equal to version III and version VI in Table I, respectively. Version III, version IV, and version V use both an RGB image and an optical flow map as motion input. Version III directly fuses them before motion encoder, model IV fuses the features before decoding, and version V fuses the final logits after decoding. Although these methods obtain some improvements on FBMS test set and YouTube-Objects dataset, the performance on the DAVIS 2016 validation set is much lower than version I. As the performance gap between version I and version II is quite large, negative influence caused by the model version II during the fusion process is not negligible. Whereas if output selection algorithm is adopted, performance degradation is not observed as only the selected optimal output is used as the final prediction.

We also report the ratio of the selected source information for motion encoder in Table IV. The selection ratio depends a lot on the testing datasets. In DAVIS 2016 validation set, RGB images are selected at only 3.78% of the total frames. By contrast, in FBMS test set and YouTube-Objects dataset, 37.6% and 38.8% of the total frames are selected, respectively. In other words, optical flow maps are very effective in the DAVIS 2016 validation set, but are less effective in the FBMS test set and YouTube-Objects dataset. This also accords with

the quantitative results in Table I and Table II that using optical flow maps as motion input is more effective on the DAVIS 2016 validation set compared to on others.

D. Quantitative Results

To compare our proposed approach to other state-of-the-art methods, we report performance on four popular benchmark datasets: DAVIS 2016 [5] validation set, FBMS [6] test set, YouTube-Objects [7] dataset, and Long-Videos [8] dataset. For a fair comparison, we also report the performance of our method with test-time augmentation if required. As the augmentation strategy, we apply multi-scale (resolution: 288, 384, 672) and flipping (horizontal) ensemble, following HFAN [4].

DAVIS 2016. In Table V, the performance on the DAVIS 2016 validation set is reported. The methods using external post-processing techniques, such as fully connected CRF [50] and instance pruning proposed in AD-Net [12], are marked for a fair comparison. Additionally, inference speed is also reported to evaluate the efficiency of the system, if available. Note that optical flow generation time and post-processing time are not considered when calculating the inference speed. From the table, D²Conv3D [48] achieves a notable performance with a \mathcal{G} score of 86.0%. However, it requires a large amount of pre-training data to learn frame-level correspondences, such as Kinetics400 [51] and Sports-1M [52]. IMP [14] also exhibits remarkable performance with a \mathcal{G} score of 85.6% only with RGB images, but it requires entire video frames to understand the sequence from a global perspective, preventing online availability. HFAN obtains the highest performance among the

TABLE VI
QUANTITATIVE EVALUATION ON THE YOUTUBE-OBJECTS DATASET. PERFORMANCE IS REPORTED WITH THE \mathcal{J} MEAN. † INDICATES THE USE OF TEST-TIME AUGMENTATION STRATEGY.

Method	Aeroplane	Bird	Boat	Car	Cat	Cow	Dog	Horse	Motorbike	Train	Mean
PDB [44]	78.0	80.0	58.9	76.5	63.0	64.1	70.1	67.6	58.4	35.3	65.5
AGS [18]	87.7	76.7	72.2	78.6	69.2	64.6	73.3	64.4	62.1	48.2	69.7
COSNet [9]	81.1	75.7	71.3	77.6	66.5	69.8	76.8	67.4	67.7	46.8	70.5
AGNN [10]	71.1	75.9	70.7	78.1	67.9	69.7	77.4	67.3	<u>68.3</u>	47.8	70.8
MATNet [1]	72.9	77.5	66.9	79.0	73.7	67.4	75.9	63.2	62.6	51.0	69.0
WCS-Net [46]	81.8	81.1	67.7	79.2	64.7	65.8	73.4	<u>68.6</u>	69.7	49.2	70.5
RTNet [15]	84.1	80.2	70.1	79.5	71.8	70.1	71.3	65.1	64.6	53.3	71.0
AMC-Net [3]	78.9	80.9	67.4	<u>82.0</u>	69.0	69.6	75.8	63.0	63.4	57.8	71.1
HFAN (MiT-b1) [†] [4]	84.7	80.0	<u>72.0</u>	76.1	76.0	71.2	76.9	71.0	64.3	61.4	<u>73.4</u>
HCPN [17]	84.5	79.6	67.3	87.8	74.1	71.2	76.5	66.2	65.8	<u>59.7</u>	73.3
TMO (RN-101) [33]	<u>85.7</u>	80.0	70.1	78.0	73.6	70.3	76.8	66.2	58.6	47.0	71.5
TMO++ (RN-101)	84.2	80.2	71.8	78.6	74.8	72.3	79.2	66.9	63.4	47.2	73.1
TMO (MiT-b1) [33]	81.8	<u>84.5</u>	68.0	77.9	74.7	67.9	78.0	65.0	56.2	49.6	71.1
TMO++ (MiT-b1)	83.2	85.0	69.6	78.1	<u>77.3</u>	70.6	80.3	64.8	61.1	50.8	73.0
TMO++ (MiT-b1)[†]	83.8	85.0	70.9	77.5	78.0	<u>71.3</u>	<u>80.2</u>	65.3	62.3	50.6	73.5

existing methods with a transformer-based backbone network, MiT-b1 [37]. However, it uses relatively high input resolution and is quite slow for real-world application. Even without post-processing techniques and maintaining online availability, our method outperforms all other methods in terms of both prediction accuracy and inference speed. Specifically, TMO [33] based on MiT-b1 achieves a \mathcal{G} score of 87.2% and an exceptionally fast inference speed of 66.7 fps.

FBMS. We report quantitative evaluation on the FBMS test set in Table V. One unique property of the FBMS dataset is that the video sequences may contain multiple salient objects that should be detected together. Among the existing methods, TransportNet [16] achieves the best performance with a \mathcal{J} score of 78.7%. Performances of HCPN [17], F2Net [13], and IMP are also impressive, showing \mathcal{J} scores of 78.3%, 77.5%, and 77.5%, respectively. With MiT-b1 backbone, our proposed TMO surpasses all other methods by a large margin, with a \mathcal{J} score of 80.0%. Additionally, if adaptive output selection algorithm is adopted on top of it, the performance further increases to 83.2%, outperforming previous best performance by 4.5%. For both ResNet-101 [36] backbone version and MiT-b1 backbone version, applying adaptive output selection significantly improves the performance of TMO.

YouTube-Objects. In Table VI, we quantitatively compare various VOS approaches on the YouTube-Objects dataset. On YouTube-Objects dataset, the model performance is evaluated using per-class accuracy that indicates the mean score of the sequences in each class, and overall accuracy that indicates the mean score of the entire sequences. Among the existing methods, HFAN with MiT-b1 backbone achieves overall \mathcal{J} score of 73.4% with test-time augmentation strategy. With the same backbone network and test-time augmentation strategy, TMO++ surpasses HFAN with overall \mathcal{J} score of 73.5%.

Long-Videos. In Table VII, we also report the performance on the Long-Videos dataset. By memorizing past frames information, memory-based approaches including STM [40] and AFB-URR [8] achieve remarkable performance on long video

TABLE VII
QUANTITATIVE EVALUATION ON THE LONG-VIDEOS DATASET. SS AND MS DENOTE SEMI-SUPERVISED AND UNSUPERVISED, RESPECTIVELY. † INDICATES THE USE OF TEST-TIME AUGMENTATION STRATEGY.

Method	Publication	Type	\mathcal{J}_M
A-GAME [54]	CVPR'19	SS	50.0
RVOS [53]	CVPR'19	SS	10.2
STM [40]	ICCV'19	SS	<u>79.1</u>
CFBI [29]	ECCV'20	SS	50.9
AFB-URR [8]	NeurIPS'20	SS	82.7
AGNN [10]	ICCV'19	US	68.3
MATNet [1]	AAAI'20	US	66.4
3DC-Seg [47]	BMVC'20	US	34.2
HFAN (MiT-b1) [†] [4]	ECCV'22	US	<u>74.9</u>
TMO (MiT-b1) [33]	WACV'23	US	71.8
TMO++ (MiT-b1)		US	74.8
TMO++ (MiT-b1)[†]		US	75.8

sequences. Among the unsupervised VOS methods, TMO++ with test-time augmentation obtains the best performance with a \mathcal{J} score of 75.8%, demonstrating its superiority in real-world scenarios. Interestingly, our method shows even better performance than some semi-supervised VOS methods that have advantages over the unsupervised VOS setting. The results demonstrate that our per-frame pipeline is effective and stable for long videos, and sometimes even better than recurrent pipeline widely used in semi-supervised VOS setting.

E. Qualitative Results

We qualitatively compare our method to state-of-the-art PMN [49] and Isomer [55] on the FBMS [6] test set in Figure 4. For a fair comparison, we compare our method to the methods that leverage motion cues obtained from estimated optical flow maps as our method. As shown in the figure, noisy results are observed in PMN and Isomer, especially when optical flow maps are confusing or unclear. As they are highly dependent on motion cues, errors of optical flow maps cannot be handled appropriately. Unlike those methods, TMO++ does



Fig. 5. Qualitative comparison of different methods on the FBMS test set.

not generate noisy or erroneous results even with confusing optical flow maps as input, as it is learned to leverage motion cues as optional and optimal source information for motion encoder is adaptively selected during inference. The qualitative results also demonstrate that our approach is more stable and reliable compared to conventional solutions.

V. LIMITATION

Although the proposed adaptive output selection algorithm is a useful tool for boosting performance of the motion-as-option network, it is not always helpful as can be found at Table III. Unlike on the FBMS [6] test set and YouTube-Objects [7] dataset, no performance improvement is observed on the DAVIS [5] 2016 validation set. This is because the DAVIS 2016 dataset is composed of high-quality and high-resolution video samples, which enables to obtain high-quality optical flow maps. As those optical flow maps are reliable in most cases, additionally using motion cues is generally more effective than using only appearance cues, as can be seen at Table IV. However, in real-world scenarios where not all videos are well taken as the DAVIS dataset, we believe that adaptive output selection can greatly increase the performance and stability of the motion-as-option network.

VI. CONCLUSION

In unsupervised VOS, the combined use of appearance and motion cues has been an effective and powerful approach.

However, existing two-stream approaches are susceptible to low-quality optical flow maps, degrading their usability and reliability for real-world usage. To relieve this concern, we propose a motion-as-option network that is not much dependent on motion cues and a collaborative network learning strategy to fully leverage its unique property. Additionally, an adaptive output selection algorithm is proposed to maximize the efficacy of the motion-as-option network at test time. On all public benchmark datasets, our approach affords a new state-of-the-art performance with real-time inference speed. We believe that our simple, fast, and strong approach can serve as a solid baseline for future VOS research.

REFERENCES

- [1] Zhou, Tianfei, et al. "Motion-attentive transition for zero-shot video object segmentation." Proceedings of the AAAI conference on artificial intelligence. Vol. 34. No. 07. 2020.
- [2] Ji, Ge-Peng, et al. "Full-duplex strategy for video object segmentation." Proceedings of the IEEE/CVF international conference on computer vision. 2021.
- [3] Yang, Shu, et al. "Learning motion-appearance co-attention for zero-shot video object segmentation." Proceedings of the IEEE/CVF international conference on computer vision. 2021.
- [4] Pei, Gensheng, et al. "Hierarchical feature alignment network for unsupervised video object segmentation." European Conference on Computer Vision. Cham: Springer Nature Switzerland, 2022.
- [5] Perazzi, Federico, et al. "A benchmark dataset and evaluation methodology for video object segmentation." Proceedings of the IEEE conference on computer vision and pattern recognition. 2016.
- [6] Ochs, Peter, Jitendra Malik, and Thomas Brox. "Segmentation of moving objects by long term video analysis." IEEE transactions on pattern analysis and machine intelligence 36.6 (2013): 1187-1200.

- [7] Prest, Alessandro, et al. "Learning object class detectors from weakly annotated video." 2012 IEEE Conference on computer vision and pattern recognition. IEEE, 2012.
- [8] Liang, Yongqing, et al. "Video object segmentation with adaptive feature bank and uncertain-region refinement." *Advances in Neural Information Processing Systems* 33 (2020): 3430-3441.
- [9] Lu, Xiankai, et al. "See more, know more: Unsupervised video object segmentation with co-attention siamese networks." *Proceedings of the IEEE/CVF conference on computer vision and pattern recognition*. 2019.
- [10] Wang, Wenguan, et al. "Zero-shot video object segmentation via attentive graph neural networks." *Proceedings of the IEEE/CVF international conference on computer vision*. 2019.
- [11] Zhen, Mingmin, et al. "Learning discriminative feature with crf for unsupervised video object segmentation." *Computer Vision—ECCV 2020: 16th European Conference, Glasgow, UK, August 23–28, 2020, Proceedings, Part XXVII 16*. Springer International Publishing, 2020.
- [12] Yang, Zhao, et al. "Anchor diffusion for unsupervised video object segmentation." *Proceedings of the IEEE/CVF international conference on computer vision*. 2019.
- [13] Liu, Daizong, et al. "F2net: Learning to focus on the foreground for unsupervised video object segmentation." *Proceedings of the AAAI Conference on Artificial Intelligence*. Vol. 35. No. 3. 2021.
- [14] Lee, Youngjo, Hongje Seong, and Euntai Kim. "Iteratively selecting an easy reference frame makes unsupervised video object segmentation easier." *Proceedings of the AAAI Conference on Artificial Intelligence*. Vol. 36. No. 2. 2022.
- [15] Ren, Sucheng, et al. "Reciprocal transformations for unsupervised video object segmentation." *Proceedings of the IEEE/CVF conference on computer vision and pattern recognition*. 2021.
- [16] Zhang, Kaihua, et al. "Deep transport network for unsupervised video object segmentation." *Proceedings of the IEEE/CVF International Conference on Computer Vision*. 2021.
- [17] Pei, Gensheng, et al. "Hierarchical Co-Attention Propagation Network for Zero-Shot Video Object Segmentation." *IEEE Transactions on Image Processing* (2023).
- [18] Wang, Wenguan, et al. "Learning unsupervised video object segmentation through visual attention." *Proceedings of the IEEE/CVF conference on computer vision and pattern recognition*. 2019.
- [19] Yang, Chuan, et al. "Saliency detection via graph-based manifold ranking." *Proceedings of the IEEE conference on computer vision and pattern recognition*. 2013.
- [20] Li, Yin, et al. "The secrets of salient object segmentation." *Proceedings of the IEEE conference on computer vision and pattern recognition*. 2014.
- [21] Cheng, Ming-Ming, et al. "Global contrast based salient region detection." *IEEE transactions on pattern analysis and machine intelligence* 37.3 (2014): 569-582.
- [22] Wang, Lijun, et al. "Learning to detect salient objects with image-level supervision." *Proceedings of the IEEE conference on computer vision and pattern recognition*. 2017.
- [23] Lin, Tsung-Yi, et al. "Microsoft coco: Common objects in context." *Computer Vision—ECCV 2014: 13th European Conference, Zurich, Switzerland, September 6-12, 2014, Proceedings, Part V 13*. Springer International Publishing, 2014.
- [24] Xu, Ning, et al. "Youtube-vos: A large-scale video object segmentation benchmark." *arXiv preprint arXiv:1809.03327* (2018).
- [25] Hastie, Trevor, et al. *The elements of statistical learning: data mining, inference, and prediction*. Vol. 2. New York: springer, 2009.
- [26] Cheng, Ke, et al. "Skeleton-based action recognition with shift graph convolutional network." *Proceedings of the IEEE/CVF conference on computer vision and pattern recognition*. 2020.
- [27] Lee, Jungho, et al. "Hierarchically decomposed graph convolutional networks for skeleton-based action recognition." *arXiv preprint arXiv:2208.10741* (2022).
- [28] Lee, Jungho, et al. "Leveraging Spatio-Temporal Dependency for Skeleton-Based Action Recognition." *arXiv preprint arXiv:2212.04761* (2022).
- [29] Yang, Zongxin, Yunchao Wei, and Yi Yang. "Collaborative video object segmentation by foreground-background integration." *European Conference on Computer Vision*. Cham: Springer International Publishing, 2020.
- [30] Xu, Xiaohao, et al. "Reliable propagation-correction modulation for video object segmentation." *Proceedings of the AAAI Conference on Artificial Intelligence*. Vol. 36. No. 3. 2022.
- [31] Cho, Suhwan, et al. "Tackling background distraction in video object segmentation." *European Conference on Computer Vision*. Cham: Springer Nature Switzerland, 2022.
- [32] Woo, Sanghyun, et al. "Cbam: Convolutional block attention module." *Proceedings of the European conference on computer vision (ECCV)*. 2018.
- [33] Cho, Suhwan, et al. "Treating motion as option to reduce motion dependency in unsupervised video object segmentation." *Proceedings of the IEEE/CVF Winter Conference on Applications of Computer Vision*. 2023.
- [34] Teed, Zachary, and Jia Deng. "Raft: Recurrent all-pairs field transforms for optical flow." *Computer Vision—ECCV 2020: 16th European Conference, Glasgow, UK, August 23–28, 2020, Proceedings, Part II 16*. Springer International Publishing, 2020.
- [35] Butler, Daniel J., et al. "A naturalistic open source movie for optical flow evaluation." *Computer Vision—ECCV 2012: 12th European Conference on Computer Vision, Florence, Italy, October 7-13, 2012, Proceedings, Part VI 12*. Springer Berlin Heidelberg, 2012.
- [36] He, Kaiming, et al. "Deep residual learning for image recognition." *Proceedings of the IEEE conference on computer vision and pattern recognition*. 2016.
- [37] Xie, Enze, et al. "SegFormer: Simple and efficient design for semantic segmentation with transformers." *Advances in Neural Information Processing Systems* 34 (2021): 12077-12090.
- [38] Krizhevsky, Alex, Ilya Sutskever, and Geoffrey E. Hinton. "Imagenet classification with deep convolutional neural networks." *Advances in neural information processing systems* 25 (2012).
- [39] Kingma, Diederik P., and Jimmy Ba. "Adam: A method for stochastic optimization." *arXiv preprint arXiv:1412.6980* (2014).
- [40] Oh, Seoung Wug, et al. "Video object segmentation using space-time memory networks." *Proceedings of the IEEE/CVF International Conference on Computer Vision*. 2019.
- [41] Seong, Hongje, Junhyuk Hyun, and Euntai Kim. "Kernelized memory network for video object segmentation." *Computer Vision—ECCV 2020: 16th European Conference, Glasgow, UK, August 23–28, 2020, Proceedings, Part XXII 16*. Springer International Publishing, 2020.
- [42] Cho, Suhwan, et al. "Pixel-level bijective matching for video object segmentation." *Proceedings of the IEEE/CVF Winter Conference on Applications of Computer Vision*. 2022.
- [43] Ioffe, Sergey, and Christian Szegedy. "Batch normalization: Accelerating deep network training by reducing internal covariate shift." *International conference on machine learning*. pmlr, 2015.
- [44] Song, Hongmei, et al. "Pyramid dilated deeper convlstm for video salient object detection." *Proceedings of the European conference on computer vision (ECCV)*. 2018.
- [45] Siam, Mennatullah, et al. "Video object segmentation using teacher-student adaptation in a human robot interaction (hri) setting." *2019 International Conference on Robotics and Automation (ICRA)*. IEEE, 2019.
- [46] Zhang, Lu, et al. "Unsupervised video object segmentation with joint hotspot tracking." *Computer Vision—ECCV 2020: 16th European Conference, Glasgow, UK, August 23–28, 2020, Proceedings, Part XIV 16*. Springer International Publishing, 2020.
- [47] Mahadevan, Sabarinath, et al. "Making a case for 3d convolutions for object segmentation in videos." *arXiv preprint arXiv:2008.11516* (2020).
- [48] Schmidt, Christian, et al. "D2conv3d: Dynamic dilated convolutions for object segmentation in videos." *Proceedings of the IEEE/CVF Winter Conference on Applications of Computer Vision*. 2022.
- [49] Lee, Minhyeok, et al. "Unsupervised video object segmentation via prototype memory network." *Proceedings of the IEEE/CVF Winter Conference on Applications of Computer Vision*. 2023.
- [50] Krähenbühl, Philipp, and Vladlen Koltun. "Efficient inference in fully connected crfs with gaussian edge potentials." *Advances in neural information processing systems* 24 (2011).
- [51] Kay, Will, et al. "The kinetics human action video dataset." *arXiv preprint arXiv:1705.06950* (2017).
- [52] Karpathy, Andrej, et al. "Large-scale video classification with convolutional neural networks." *Proceedings of the IEEE conference on Computer Vision and Pattern Recognition*. 2014.
- [53] Ventura, Carles, et al. "Rvos: End-to-end recurrent network for video object segmentation." *Proceedings of the IEEE/CVF conference on computer vision and pattern recognition*. 2019.
- [54] Johnder, Joakim, et al. "A generative appearance model for end-to-end video object segmentation." *Proceedings of the IEEE/CVF conference on computer vision and pattern recognition*. 2019.
- [55] Yuan, Yichen, et al. "Isomer: Isomeric Transformer for Zero-shot Video Object Segmentation." *arXiv preprint arXiv:2308.06693* (2023).